Minor species in Venus' night side troposphere as observed by VIRTIS-H/Venus Express

Emmanuel Marcq, B. Bézard, J.-M. Reess, F. Henry, S. Érard, S. Robert, Franck Montmessin, Franck Lefèvre, Maxence Lefevre, A. Stolzenbach, et al.

Minor species in Venus' night side troposphere as observed by VIRTIS-H/Venus Express

E. Marcq[1], B. Bézard[2], J.-M. Reess[2], F. Henry[2], S. Érard[2], S. Robert[3], F. Montmessin[1], F. Lefèvre[1], M. Lefèvre[1], A. Stolzenbach[4], J.-L. Bertaux[1], G. Piccioni[5], P. Drossart[6]

[1]LATMOS/IPSL, UVSQ Université Paris-Saclay, Sorbonne Université, CNRS, Guyancourt, France
[2]LESIA, Observatoire de Paris, Université PSL, CNRS, Sorbonne Université, Université Paris-Cité, Meudon, France
[3]Royal Belgian Institute for Space Aeronomy, Brussels, Belgium
[4]Instituto de Astrofisica de Andalucia, Granada, Spain
[5]Istituto di Astrofisica Spaziale e Fisica Cosmica (IASF) - Istituto Nazionale di Astrofisica (INAF), Roma, Italy
[6]Institut d'Astrophysique de Paris, Sorbonne Universités, CNRS, Paris, France

Key Points:

- The latitudinal variability of carbon monoxide on Venus is confirmed, as well as its anti-correlation with carbonyl sulfide.
- Zonal variations of carbon monoxide near the equator may be correlated with zonally shifted surface elevation.
- No variations of water vapor and sulfur dioxide were found; a spectral resolving power nearing 10000 is needed to further investigate.

Corresponding author: Emmanuel Marcq, `emmanuel.marcq@latmos.ipsl.fr`

Abstract

The 2.3 µm spectral window has been used to constrain the composition of the lower atmosphere (in the 30-40 km altitude range) on the night side of Venus for more than thirty years. Here, we present a follow-up study of Marcq et al. (2008), but using the full VIRTIS-H/Venus Express data archive as well as an updated radiative transfer forward model. We are able to confirm a latitudinal increase of CO of about 30% between 0° and 60°N, as well as an anti-correlated vertical shift of OCS profile by about −1 km in the same latitude range. Both variations are about twice smaller in the southern hemisphere. Correlations of low latitude CO and OCS variations with zonally shifted surface elevation is tentatively found. These results are consistent with CO and OCS variations resulting from the competition between local thermochemistry and a Hadley-cell-like general circulation, albeit influenced by the orography. Finally, no evidence for spatial variations of water vapor (combined H_2O and HDO) or sulfur dioxide could be evidenced in this data set; better constraining possible variations of these species would require future missions to include infrared spectrometers operating at a spectral resolving power higher than $\sim 10^4$, such as VenSpec-H onboard EnVision.

Plain Language Summary

Remotely measuring the composition of the Venusian atmosphere below the clouds is challenging, yet yields invaluable insights about the atmospheric chemistry, circulation and interaction with the surface and interior of the planet. The VIRTIS-H instrument on board ESA's *Venus Express* orbiter (2006-2014) provides a rich data set in this regard, thanks to its ability to observe and analyse, on the night side of the planet, the infrared radiation emitted by the deep atmospheric layers. The results of our analyses confirm the previously observed trends for the variations of two trace gases (carbon monoxide and carbonyl sulfide) with latitude, explained by the combined effects of chemical reactions and transport by the atmospheric circulation. Variations of carbon monoxide may also be linked to the variations of ground elevation, confirming the link between surface topography and atmospheric circulation. However, we were unable to separate the signature of heavy water vapor from ordinary water vapor or to detect any variations in sulfur dioxide, both of which require more powerful infrared instruments such as those planned on future Venus orbiters such as ESA's EnVision.

1 Introduction

Since its serendipitous discovery by Allen and Crawford (1984), the 2.3 µm night side emission of Venus has proven an invaluable tool to investigate the tropospheric chemistry and the lower cloud deck. Its thermal origin from atmospheric layers located between 30 and 40 km in altitude, below the clouds, was already suspected by Allen (1987), and its first radiative transfer modelings (Crisp et al., 1989; Bézard et al., 1990) have shown that numerous trace gases could be measured in this region: H_2O, HDO, HF, SO_2, OCS and CO. For CO and OCS, the variation of their peak contribution functions within the spectral window was extended enough so that not only their mean abundance, but also their vertical gradient could be retrieved (Pollack et al., 1993).

Ground based observations at a high spectral resolution could even constrain the global average value of sulfur dioxide in the 30-40 km altitude range (Bézard et al., 1993; Marcq et al., 2021) as well as of the isotopic ratio of deuterium in water vapor (de Bergh et al., 1991, 1995), and found a value about 100 times higher than on Earth, with strong implication on the past history of water (Grinspoon, 1993). Conversely, early space borne observations made use of relatively low spectral resolution instruments such as NIMS/Galileo (Carlson et al., 1991; Collard et al., 1993) during its Venus fly-by. Such observations could only constrain the broadest spectral signature of CO (2-0 rovibrational band), but at a spatial resolution unachievable from Earth. In consequence, they were able to detect the latitudinal increase of CO from the lower to the higher latitudes, a feature that was confirmed by VIRTIS-M (Tsang et al., 2008, 2009; Haus et al., 2015; Tsang & McGouldrick, 2017) at a similar spectral resolution in the same spectral window, but on board the orbiter *Venus Express* (Drossart et al., 2007; Titov et al., 2006). They were thus able to map tropospheric CO abundance over the whole night side, with some hints of zonal variations, and provided a physical interpretation of these variations based on the competition between large scale Hadley cell-like vertical circulation and the existing vertical gradient of CO required by thermochemical equilibrium. In between, moderate ($500 < \lambda/\Delta\lambda < 5000$) spectral resolution observations were performed from both Earth-based telescopes (Marcq et al., 2005, 2006; Cotton et al., 2012; Arney et al., 2014) and from VIRTIS-H on board *Venus Express* (Marcq et al., 2008). These observations give access to the spatial variability of more trace species (CO, but also OCS and H_2O; even SO_2 to a limited extent) than low ($\lambda/\Delta\lambda < 500$) spectral resolution observations, at a cost of a lower spatial resolution and/or coverage. They confirmed the spatial variability of

CO on planetary scales, and also found anti-correlated variations of OCS, but no evidence for any variability for H_2O or SO_2.

Here we present an update to the first VIRTIS-H 2.3 µm study performed by Marcq et al. (2008), with two major differences: (1) whereas Marcq et al. (2008) used a selection data from the first 298 orbits of *Venus Express*, we use the whole extent of VIRTIS-H data acquired during the science mission as detailed in Sec. 2; and (2) the forward radiative transfer model and retrieval algorithms have undergone significant updates as detailed in Sec. 3. Measurements of tropospheric minor species (CO, OCS, water vapor, SO_2) and their variability according to latitude, longitude and/or local solar time are presented in Sec. 4, and discussed in the context of coupled chemistry and dynamics in Sec. 5. Implications for the design of future instrumentation can be found in the last Sec. 6.

2 Observational data set

2.1 Global coverage

In order to extend the study from Marcq et al. (2008), we downloaded from ESA's Planetary Science Archive (PSA) the whole VIRTIS-H night side data set calibrated in physical units along the provided observational geometry information. We selected all files whose local solar time range intersects the 7pm-5am interval, leaving an hour of local solar time margin in order to avoid cross-terminator scattering of sunlight by the upper clouds and hazes – the spectral radiance of day side Venus near 2.3 µm being about three orders of magnitude larger than the spectral radiance of the night side thermal emission (Titov et al., 2018).

Successful observations were defined as yielding a relative accuracy better than 10% for carbon monoxide, which is the easiest species to retrieve; a criterion solely based on signal-to-noise ratio would fail to reject some observations of poor quality due remaining uncorrected biases (e.g. faulty straylight correction). They are shown in Fig. 1. Several remarks and comments can be inferred. First of all, latitudinal coverage is very good between ±60° in latitude, but is very sparse beyond these values. This is caused by the thicker lower clouds at higher latitudes (in both north and south pole collars and vortices) which drastically decreases the signal-to-noise ratio and therefore does not allow for fitting and retrieving minor species.

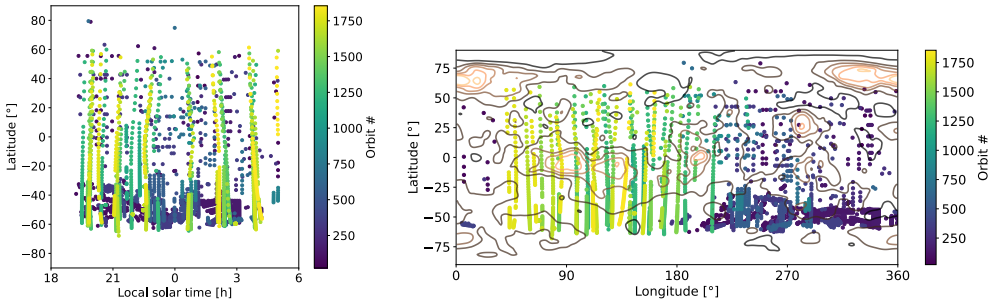

Figure 1. Location of the 3143 successful observations in local solar time/latitude (left) and longitude/latitude (right) coordinates. Color codes for the orbit number. Brown contours in the rightmost map stands for topographic elevation at −1, 0, 1, 2, 3 and 4 km following the Magellan-based digital elevation model used by Lebonnois et al. (2010).

Secondly, both local solar times and planetocentric longitudes are well sampled in our data set, albeit with a major difference: there is no correlation between the observation date and their local solar time, whereas there is a strong correlation between the observation date and their longitude. The latter is caused by the slowly precessing quasi-polar orbit of *Venus Express* combined with the relatively short lifetime of VIRTIS-H (operating from 2006-05-14, first available orbit # 23, until 2011-06-21, last available orbit # 1888) which prevented re-visit of previously observed longitudes. This should be kept in mind when discussing our results, since any trend seen with respect to observation date could also be ascribed to longitudinal variations (and conversely). Such an issue was already pointed out in the analysis of other data sets from other *Venus Express* instruments such as VMC or SPICAV (Khatuntsev et al., 2013; Bertaux et al., 2016; Marcq et al., 2020).

Finally, it can also be noted that we have more sampled points in the southern hemisphere than in the northern hemisphere, due to the high northern latitude of the pericentre of *Venus Express*, yet the extensive coverage of this study constitutes a real improvement over our previous study (Marcq et al., 2008).

2.2 Data processing

VIRTIS-H was the infrared high spectral resolution channel of the VIRTIS instrument (Coradini et al., 1998). Its optical design consisted in an echelle grating spectrometer, with 7 diffraction orders covering the 2-5 µm range focused on the detector plane.

The spectral resolving power varied from 1500 to 2500, according to the diffraction order and the 432 discrete channels of each order, as shown by Marcq et al. (2008) (their Fig. 1). The spectral range of 3 among these diffraction orders intersected the 2.3 μm spectral window and are used hereafter: orders 5 (2.19-2.73 μm), 6 (2.00-2.50 μm) and 7 (1.85-2.31 μm).

The first step of processing for these 3 diffraction orders is to correct for an even-odd effect by removing the spurious oscillating component through simple 2-pixel wide window averaging. Then, second degree polynomial adjustment is applied to the provided wavelength assignment function (pixel number to physical wavelength), based on the distinctive spectral features seen in observations as well as in the forward model (Sec. 3.1).

2.2.1 Zero-level adjustment

As shown in (Marcq et al., 2008), a correction must be applied in order to set the proper zero-level for each relevant diffraction order (most likely caused by unperfect straylight correction). We can take advantage here of the fact that orders 5 and 7 both include part of the 2.3 μm window and part of the spectral interval where CO_2 continuum opacity leads to a negligible thermal emission. Thus, the average of order 5 spectra for wavelengths larger than 2.65 μm provides a good estimation of the true zero level for order 5, and so does the average of order 7 spectra for wavelengths ranging between 2.12 and 2.17 μm (the imperfect straylight correction at wavelengths shortwards of 2.12 μm is not good enough for their inclusion). Order 6 does encompass the whole 2.3 μm window, but does not include significant contributions outside of these windows. Therefore, we have to use here a linear interpolation (with respect to wavelength) between the short-end zero level found with order 7 and the long-end zero-level found with order 5. Also, since order 7 only includes the CO_2-dominated part of the 2.3 μm window, it is only used for deriving the zero level for order 6 as stated above. We refer the reader to the Fig. 2 in Marcq et al. (2008) for a graphical illustration.

Finally, we perform a binning between 30 consecutive spectra, yielding a typical footprint of several hundreds of kilometers, as a trade-off between the signal-to-noise ratio value, and accuracy of the observed geographical location (mainly latitude due to the aforementioned polar orbit of *Venus Express*). The minimal binned Signal-to-Noise ratio (SNR) required for a valid spectral inversion (previously defined as the successful fit-

ting of carbon monoxide abundance with a relative accuracy better than 10%, see Sec. 3.3 for details about the spectral inversion) ranges from 20 to 50, which corresponds to a SNR between 4 and 10 for an individual unbinned spectrum.

3 Methods

3.1 Radiative transfer model

The line-by-line forward radiative transfer model we use is the same as used by Marcq et al. (2021), which in turn is an update of the model used in our first analysis of VIRTIS-H spectra (Marcq et al., 2008) and described in previous work (Marcq et al., 2005, 2006). More precisely, our previous CO_2 line database from HITEMP has been updated according to the ab initio list from Huang et al. (2014) – keeping the same sub-Lorentzian parametrization as in Pollack et al. (1993)) – and our former two stream custom radiative transfer equation solver has been replaced by DISORT (Stamnes et al., 1988) in the eight-stream approximation. This allows us to include the effect of emission angle on the thermal spectra (i.e. limb darkening) at a reasonable computation cost – tests using more than 8 streams did not yield significant improvements in our computations, considering the simple analytic scattering phase functions that we use and the near-nadir observation geometry in our data set, with emission angles never exceeding 30°.

The atmosphere is divided into 90, 1-km thick plane-parallel layers from the surface up to 90 km. The temperature vs. pressure profile is kept constant according to the standard VIRA profile (Seiff, 1983), since this profile does not vary significantly below the clouds (in the 30-40 km altitude range most contributing to the thermal emission) within the investigated latitude and/or local solar time ranges (see Sec. 2.1). Clouds are modeled according to Crisp (1986), using a four modes size distribution (1,2,2',3) as described in Crisp et al. (1989) and Henyey-Greenstein scattering phase functions. Line opacities from CO_2, CO, H_2O, HDO, OCS, SO_2 and HF are extracted from (Jacquinet-Husson et al., 2011) except for CO_2 (Huang et al., 2014) as previously stated. Finally, we also have updated the (constant over the whole 2.3 µm window) value of the CO_2 continuum opacity, from our previous value of 3.5 to $2.7{\cdot}10^{-8}\,\mathrm{cm}^{-1}\cdot\mathrm{amagat}^{-2}$, which allowed for a better fit of the CO_2-dominated spectral range from 2.2 to 2.3 µm.

3.2 Fitted parameters

3.2.1 Cloud opacity

In order to account for brightness variations that affect the whole 2.3 µm spectral window (see Fig. 3), we chose to fit the lower cloud opacity through a multiplicative factor applied to the particles' number densities in the 48-57 km altitude range. This is consistent with the observed morphology of the night side thermal emission contrasts (Carlson et al., 1991; Peralta et al., 2019) coming from lower clouds opacity variations. These night side IR contrasts differ noticeably from the contrasts observed on the day side in the UV range (Markiewicz et al., 2007; Yamazaki et al., 2018), and originating from the upper clouds.

Arney et al. (2014) accounted for the cloud opacity variations in the same way, and also fitted the sulfuric acid concentration in the droplets. This was made possible by the fact they analyzed simultaneous and colocated 1.74 µm and 2.3 µm observations, therefore constraining a much larger wavelength range compared to the VIRTIS-H observations which can only encompass the 2.3 µm window alone. Therefore, we assumed a constant value for H_2SO_4 concentration in the droplets at 75% (Hansen & Hovenier, 1974).

3.2.2 Minor gaseous species

Our radiative transfer code implements vertical profiles for gaseous species by specifying a limited number of control points defined in terms of pressure P and volume mixing ratios q, and interpolating linearly $\log q$ with respect to $\log P$ between these control points, similarly to Pollack et al. (1993). The vertical location of these control points is unchanged compared to our previous studies (Marcq et al., 2005, 2006, 2008), and is readily visible in Fig. 2.

Carbon monoxide (CO), water vapor (H_2O and HDO) and sulfur dioxide (SO_2) vertical profiles are assumed to vary using a simple multiplicative constant applied to their volume mixing ratios for each control point. Hydrogen fluoride (HF) is included, but not fitted due to the narrowness of its spectral lines, which are unresolved at VIRTIS-H spectral resolution.

3.2.2.1 Carbonyl sulfide On the other hand, carbonyl sulfide (OCS) exhibits a strong vertical gradient in the 30-40 km altitude range where its contribution function

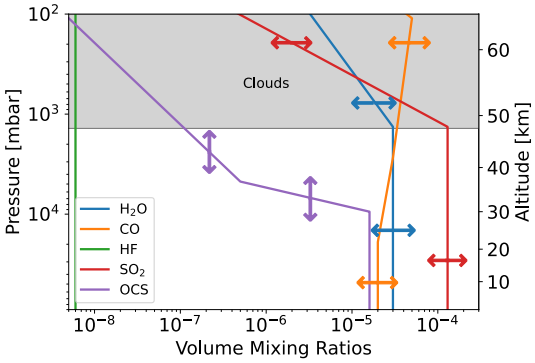

Figure 2. Nominal vertical profiles of gaseous minor species used by the forward radiative transfer model. The arrows show how these profiles are varied to fit the observed VIRTIS-H spectra.

peaks, so that we should in principle fit both its average value and vertical gradient (Pollack et al., 1993). Our attempts to improve their determination of the vertical gradient by fitting the variations of both OCS vertical gradient and VMR simultaneously were unsuccessful (degeneracy issues with OCS mixing ratio), probably due to the insufficient spectral resolution of both orders 5 and 6.

We could have adopted the same mixing ratio multiplication as for other minor species, as done by Arney et al. (2014), but it yielded comparatively poorer fits. It appears indeed that we had a better fit by vertically translating the OCS reference profile (considering we had to restrict ourselves to a single fitted parameter). More specifically, we vertically move the control points by applying a constant multiplicative factor to the pressure of the control points rather than to the mixing ratios as we did for other minor species – multiplying the pressure by $(1 + \alpha)$ is locally equivalent to a vertical translation by $-\alpha H$ where H is the local atmospheric scale height as defined by the dimensionless hydrostatic equilibrium equation: $dP/P = -dz/H$.

Such a parametrization is physically sensible, since previous studies (Tsang et al., 2008; Marcq & Lebonnois, 2013) have interpreted tropospheric variations of minor species (including OCS) as resulting from a competition between local chemical processes and updrafts/downdrafts associated with the meridional-vertical circulation. Alternatively, we could adopt the same parametrization for other minor species but this was deemed too complex for those other species since their relative vertical gradient – defined as $\Delta(\log q)/\Delta(\log P)$ – is not as large as that of OCS.

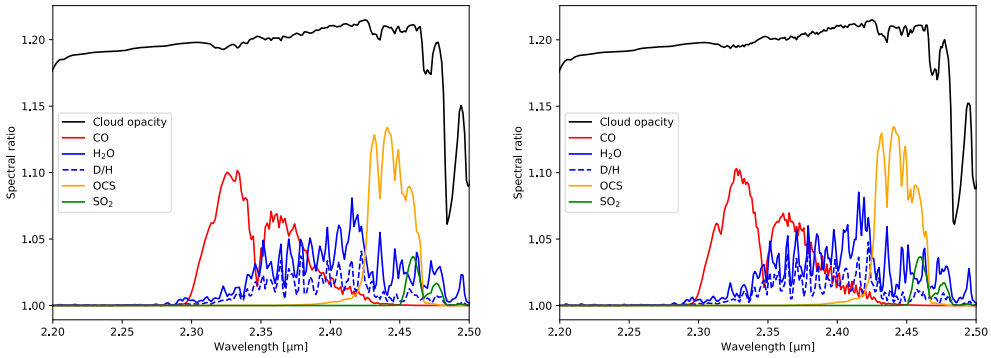

Figure 3. Synthetic spectral ratios convolved by instrumental PSF for orders 5 (left) and 6 (right) corresponding to a 10% relative difference in the atmospheric parameters described in Sec. 3.2. The small difference between both orders is due to their different PSF (see Fig. 4).

3.3 Fitting algorithm

Figure 3 shows the various spectral ranges affected by altering the vertical profiles of the aforementioned minor species, dividing synthetic spectra with a 10% variation in the above described atmospheric parameters (i.e. lower cloud opacity, multiplicative factor for gaseous species profiles) by our reference nominal synthetic spectrum. Our fitting strategy takes advantage of these different spectral ranges sequentially as follows:

1. Pre-computation of look-up tables of high-resolution spectra ($0.5\,\mathrm{cm}^{-1}$) encompassing the variation range found in observations: {cloud opacity, CO} ; {cloud opacity, CO, H_2O, HDO} ; {cloud opacity, CO, OCS, SO_2}.
2. Convolution according to the instrumental point spread function (PSF) for orders 5 and 6. A simple Gaussian convolution function would not yield satisfactory results, so we had to resort to custom, non-analytical PSF derived from ground based instrumental characterizations (Fig. 4).
3. Fit of lower cloud opacity **and** CO mixing ratio through multilinear interpolation over the convolved look-up table. The used spectral interval can be found in Table 1.
4. Fit of H_2O **or** HDO mixing ratio through multilinear interpolation over the convolved look-up table. Cloud opacity and CO mixing ratios values found previously are kept the same. The used spectral interval can be found in Table 1.
5. Fit of OCS shift altitude and SO_2 mixing ratio through multilinear interpolation over the convolved look-up table. The cloud opacity and CO values found previ-

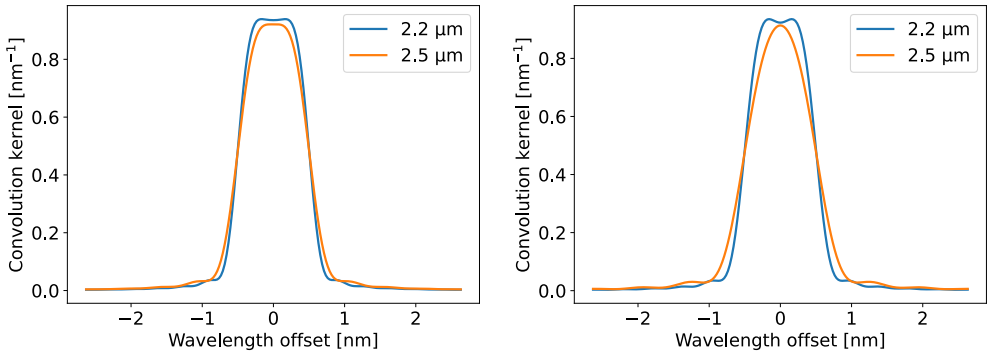

Figure 4. Normalized PSF shapes for order 5 (left) and 6 (right) for extremal wavelengths within the 2.3 µm window.

Fitted parameters	Wavelength ranges [µm]	Order(s) used
Cloud opacity, CO	2.25 – 2.28; 2.3 – 2.365; 2.4 – 2.41; 2.48 – 2.50	6
H_2O, HDO	2.345 – 2.415	5, 6
OCS, SO_2	2.38 – 2.52	5, 6

Table 1. Wavelength ranges and VIRTIS-H diffraction orders used by the fitting algorithm.

ously is kept the same (since no variations of water vapor are found compared to the nominal profile, there is no need to take its variations into account). The used spectral interval can be found in Table 1.

The values given in Table 1 deserve some comments. First, fitting the cloud opacity requires a large wavelength coverage since it affects the whole spectral window, hence the large dispersion of used wavelengths intervals used. Second, for CO and cloud opacity, the need for wavelengths shorter than 2.3 µm prevented us from using order 5 (which cannot be used for quantitative retrievals at wavelengths shorter than 2.3 µm), so that we used only order 6 to retrieve them. The use of a single order does not hamper the accuracy of these fits, since CO absorption rovibrational band and cloud opacity are the two most salient features of the 2.3 µm windows and can be fitted even at a very low spectral resolution such as VIRTIS-M (Tsang et al., 2008; Tsang & McGouldrick, 2017).

As for the two remaining fitting steps, both orders 5 and 6 were considered simultaneously when computing the χ^2 cost function to be minimized. If no single value of the parameters could fit the spectra obtained with both orders simultaneously, it led to

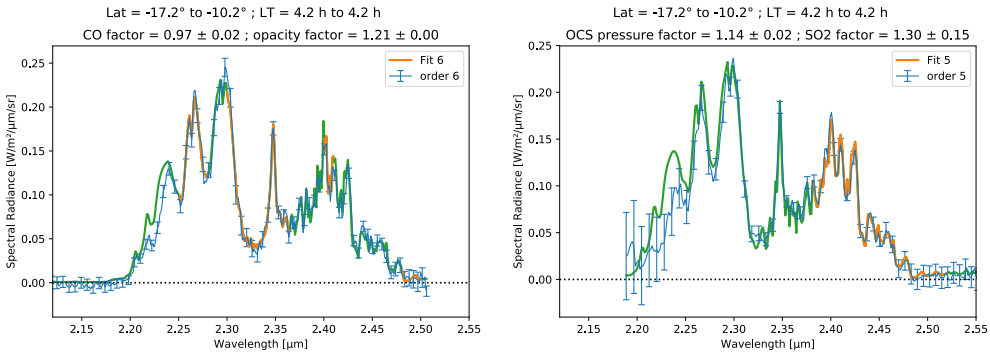

Figure 5. Best fits obtained during orbit # 277 for CO & cloud opacity with order 6 (left), and OCS & SO_2 with order 5 (right). Fitted intervals from Table 1 are shown in orange for the best fits, non-fitted intervals are shown in green for the best fits, and observed binned spectra along their 1σ error bars are shown in blue.

a poor accuracy of the fitted parameters, which can be filtered out as faulty in a second step. The χ^2 minimizer used the Levenberg-Marquardt iterative algorithm implementation from Newville et al. (2022). Examples of such fits on both orders are shown in Fig. 5. The agreement with observational data is good except in the 2.2-2.3 µm interval dominated by the poorly constrained CO_2-CO_2 absorption.

Emission angle is not included as a dimension in the computed look-up tables, since its influence on the whole spectral windows was found to be very close to the analytical parametrization that we already used in Marcq et al. (2021), namely $I(\mu) = [0.26 + 0.74\mu]\, I(0)$ where μ stands for the cosine of the emission angle. Finally, constant scaling coefficients for orders 5 and 6 were let as free parameters in the fitting routine, to account for slight residual differences in their respective absolute calibrations.

4 Results

4.1 Carbon monoxide (CO)

4.1.1 Latitudinal profile

The most robust feature of carbon monoxide distribution below the clouds of Venus is a permanent latitudinal gradient, first evidenced by NIMS/Galileo (Collard et al., 1993) and confirmed by all spectroscopic observations since then – see Marcq et al. (2018) for a detailed review of primary references. Fig. 6 displays our retrievals of carbon monox-

ide with respect to latitude, which confirms these previous observations with a minimum of 27 ± 2 ppmv (at 36 km) for latitudes below $\pm 20°$ up to a maximum of 35 ± 2 ppmv near a latitude of $+50°$, with statistical standard deviation and 1σ random accuracy being similar.

These mixing ratio values are about 3 ppm higher than in our first analysis, which can be ascribed to either a secular increase, longitudinal variations (see Sec. 4.1.2) and/or to our updates in our radiative transfer model (see Sec. 3.1), more specifically it may be caused by our update from a 2-stream radiative transfer solver to an 8-stream model. Further investigations are needed to explain this discrepancy. In any case, this underlines the fact that spectroscopic measurements are more suited to constrain variations rather than absolute mixing ratios, since the latter depend more on the assumptions made by the radiative transfer model (Bézard et al., 2009).

Interestingly, we see some evidence for north-south asymmetry, with a latitudinal gradient less steep in the southern hemisphere compared to the northern one, as well as a slight offset of the minimum in the $-20°/+10°$ latitude range. These details are very reminiscent of the 2009 observations from Arney et al. (2014), and will be discussed later in Sec. 5. We also have a larger dispersion of measurements in the southern hemisphere, but it is impossible to tell whether it is genuine or whether it results from our more extensive sampling and/or smaller footprints in the southern hemisphere, first mentioned in Sec. 2.1.

4.1.2 Other variabilities

Thanks to the extensiveness of our data set, we can investigate the variability of carbon monoxide with respect to other variables, restricting to latitudes below $\pm 20°$ in order to exclude any contamination by the well-documented latitudinal variability (Sec. 4.1.1). No significant variability with respect to local solar time was found, in contrast with the findings of Tsang and McGouldrick (2017) using VIRTIS-M, who found elevated values for CO between 10pm and 3am near the equator. However, using VIRTIS-H we could not observe the highest latitudes, where they also reported a ~ 2 ppmv dusk enhancement in CO, due to insufficient signal-to-noise.

Some low-latitude CO variability with longitude might be present in Fig. 7, with maximal values between 0 and 100° about 8 ppmv higher than the minimal values near

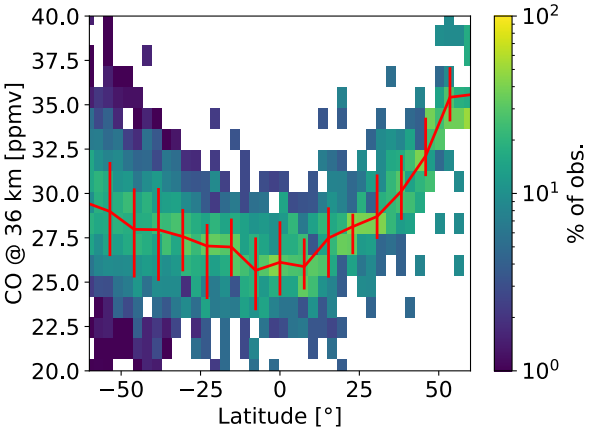

Figure 6. Carbon monoxide mixing ratios at 36 km with respect to latitude. The color code reflects the percentage of retrievals in the corresponding CO mixing ratio bin relative to all retrievals in the same latitudinal bin. The red curve stands for the moving median, and red bars represent the $\pm 1\sigma$ statistical dispersion around the median.

a longitude of 300°. An alternate interpretation would be that we observe a secular increase of CO between 2006 and 2011, since we are unable to disentangle both variables (see Sec. 2.1). Although this interpretation seems less likely, such an increase would help us to reconcile our comparatively high estimates of CO, since the CO mixing ratio values we report for first 250 orbits – which were the only ones processed at the time of Marcq et al. (2008) – are indeed similar to those reported by Marcq et al. (2008). This would imply that their estimates were not fully representative of the longitudinal/temporal average, due to insufficient longitudinal/temporal coverage.

4.2 Carbonyl sulfide (OCS)

4.2.1 Latitudinal variations

Carbonyl sulfide has been found to exhibit some degree of anticorrelation with carbon monoxide from various ground based observations (Marcq et al., 2005, 2006; Arney et al., 2014) at a spectral resolution similar to ours. The latitudinal variations of OCS are shown in Fig. 8. A downward shift of about 1 ± 0.3 km of the OCS reference profile is found at 50°N compared to the equatorial value. Since a downward vertical shift of the OCS reference profile results in a decrease in OCS mixing ratio for a given altitude in the 30-40 km range, we are therefore able to confirm the latitudinal anti-correlation

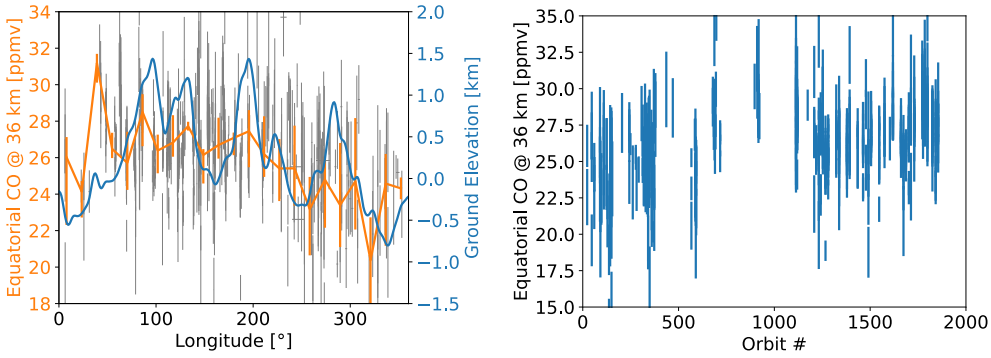

Figure 7. Carbon monoxide mixing ratios at 36 km with respect to surface longitude (left) and VEx orbit number (right), in both cases restricted to latitudes below ±25°. Error bars stand for 1σ random uncertainties. The meridional (latitudes below ±25°) average of topographic elevation according to Magellan-based digital elevation model used by Lebonnois et al. (2010) is also shown on the left.

between CO and OCS. Even the detailed features seen for CO latitudinal variations (Sec. 4.1.1) are found for OCS too: north-south asymmetry, maximal shift values in the $-20°/+10°$ latitude range, giving further credence to the CO/OCS anti-correlation.

Also, the anti-correlation is stronger compared to the one previously evidenced by e.g. Marcq et al. (2008)[their Fig. 6] where OCS was fitted through a simple multiplicative parameter. This strongly implies that this vertical shift does a better job to parameterize OCS variability with a single parameter.

4.2.2 Other variabilities

Considering the latitudinal anti-correlation between CO and OCS, one would expect the same anticorrelation to prevail between CO and OCS when plotted against longitude, solar time, date, etc. In contrast, Fig. 9 shows a correlation pattern with longitudinal elevation, and/or a possible increase with increasing date. Both would make CO and OCS shift altitude positively correlated with respect to secular variations. Hypotheses regarding these behaviors will be discussed and detailed in Sec. 5.

4.3 Water vapor (H_2O, HDO)

Our first attempt was to fit both H_2O and HDO mixing ratio separately, thereby measuring also the D/H isotopic ratio of water vapor, known to be much higher than

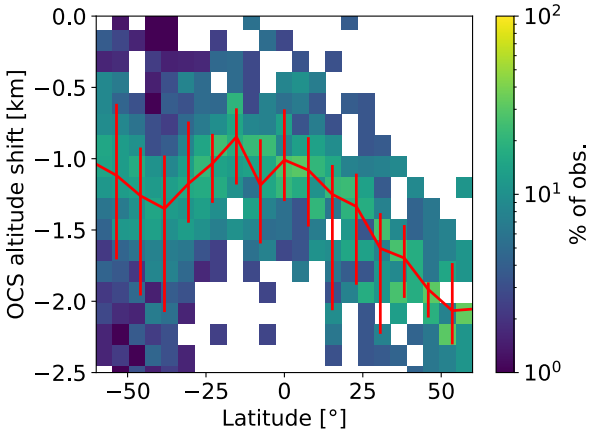

Figure 8. Vertical shift of OCS reference profile with respect to latitude. Color codes for the percentage of retrievals in the corresponding OCS vertical shift bin relative to all retrievals in the same latitudinal bin. The red curve and error bars represent the $\pm 1\sigma$ statistical dispersion around the median.

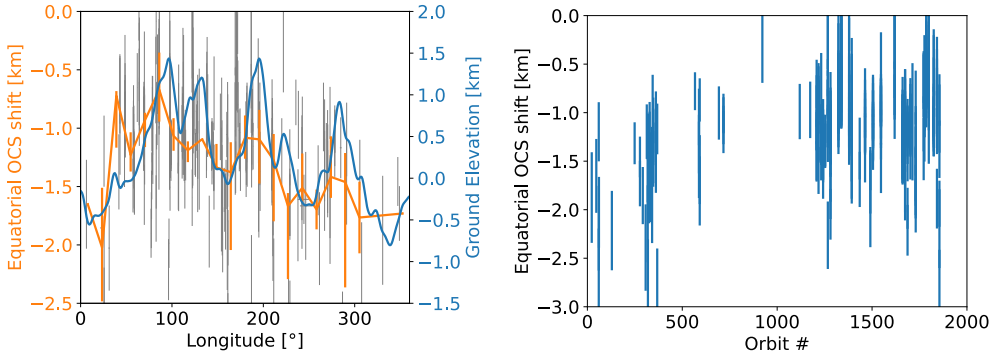

Figure 9. Carbonyl sulfide altitude shift with respect to surface longitude (left) and VEx orbit number (right), in both cases restricted to latitudes below $\pm 25°$. Error bars stand for 1σ random uncertainties. The meridional (latitudes below $\pm 25°$) average of topographic elevation according to Magellan-based digital elevation model used by Lebonnois et al. (2010) is also shown on the left.

the terrestrial value (de Bergh et al., 1991) at about 130±40 SMOW (standard mean ocean water). Unfortunately, VIRTIS-H spectral resolution is not sufficient to achieve this, and a strong degeneracy was observed between H_2O and D/H retrievals, spanning a large interval (D/H ratio between 125±50, H_2O mixing ratio between 30±10 ppmv at 35 km). To further proceed, we (1) assumed a constant D/H ratio of 130 and fit total water vapor (H_2O + HDO) mixing ratio; or (2) assumed a constant water vapor mixing ratio at 30 ppmv (Marcq et al., 2018) and fit D/H ratio. Both results are shown in

Fig. 10 according to latitude. The latitudinal average is 27±3.5 ppmv for water vapor mixing ratio, and 95±25 for D/H ratio, in agreement with previous measurements, as well as with measurements obtained at lower altitude (Bézard et al., 2011; Fedorova et al., 2015) confirming that water vapor is well mixed in the troposphere.

1σ error bars yielded by the fitting algorithm are very close to the observed standard deviation, which indicates that no significant trend in space or time can be inferred from our data set. Some hint of latitudinal variability might exist for water vapor mixing ratio (with a very weak equatorial maximum as seen in Fig. 10) although it would need further observations to be confirmed since it is below significance level with VIRTIS-H accuracy.

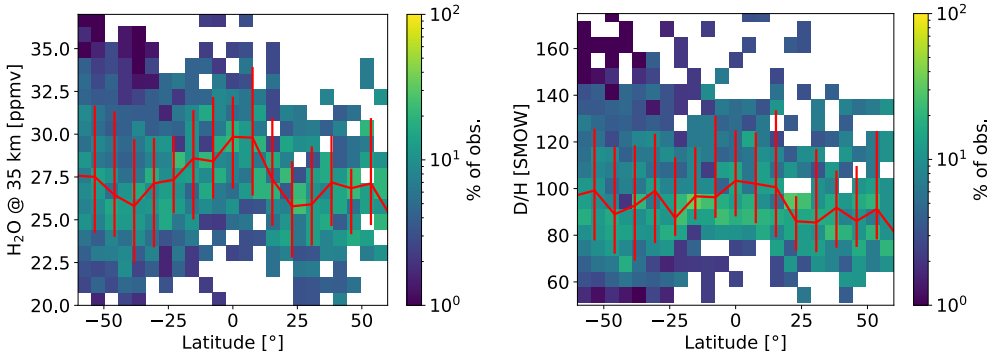

Figure 10. H_2O volume mixing ratio when assuming a constant D/H ratio of 130 (left) and D/H ratio assuming a constant water vapor mixing ratio of 30 ppmv (right) with respect to latitude. Color codes for the percentage of retrievals in the corresponding H_2O (left) and D/H (right) bin relative to all retrievals in the same latitudinal bin. The red curve and error bars represent the $\pm 1\sigma$ statistical dispersion around the median.

4.4 Sulfur dioxide (SO_2)

Our sulfur dioxide retrievals with respect to observed latitude are shown in Fig. 11. The average mixing ratio we find is 190±40 ppmv near 35 km, somewhat higher than the commonly accepted value 130 ± 50 ppmv (Arney et al., 2014; Marcq et al., 2018), although in agreement with the latest iSHELL observations (Marcq et al., 2021), which made use of a very similar radiative transfer model and retrieval algorithm. However, the same caveats as in our relatively high mixing ratios retrieved for CO also apply here, so that variations are better constrained than absolute mixing ratios. Unfortunately, the

relatively poor accuracy ($\sim 20\%$) of these SO_2 retrievals does not allow us to confirm the latitudinal trend evidenced by Marcq et al. (2021), which highlights the necessity of a much higher spectral resolution to fully explore SO_2 variability below the clouds. Similarly to what we reported in Sec. 4.3 for water vapor, 1σ error bars yielded by the fitting algorithm for SO_2 are very close to the observed standard deviation, which indicates that no significant trend in space or time can be inferred from our data set.

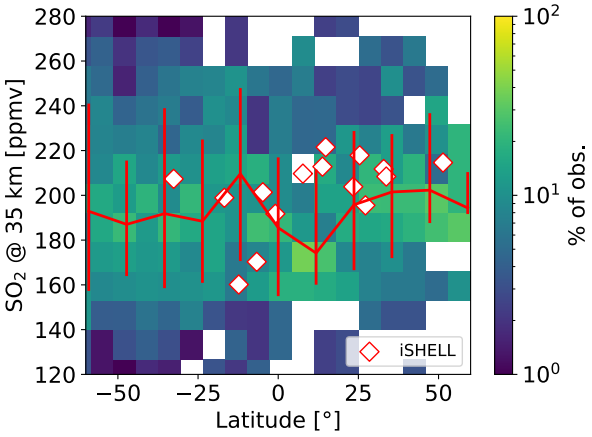

Figure 11. SO_2 volume mixing ratio with respect to latitude. Color codes for the percentage of retrievals in the corresponding SO_2 bin relative to all retrievals in the same latitudinal bin. The red curve and error bars represent the $\pm 1\sigma$ statistical dispersion around the median. Diamonds show the iSHELL retrievals from Marcq et al. (2021).

5 Interpretation

5.1 General framework

The classical interpretation of the latitudinal gradient observed for CO and OCS (Tsang et al., 2009; Tsang & McGouldrick, 2017) can be summarized as follows: for minor species which exhibit a significant vertical gradient in the probed layers (such as CO, and even more so OCS), their mixing ratio variations at planetary scale result mainly from a competition between vertical advection (driven by general circulation) and local chemical process which counterbalances this dynamical offsets. Within this framework, the latitudinal variations we have measured for CO and OCS (Sec. 4.1.1 and 4.2.1) are consistent with upwelling at lower latitudes and conversely downwelling at higher latitudes, so a Hadley-cell type circulation as expected from general circulation models (Lebonnois et

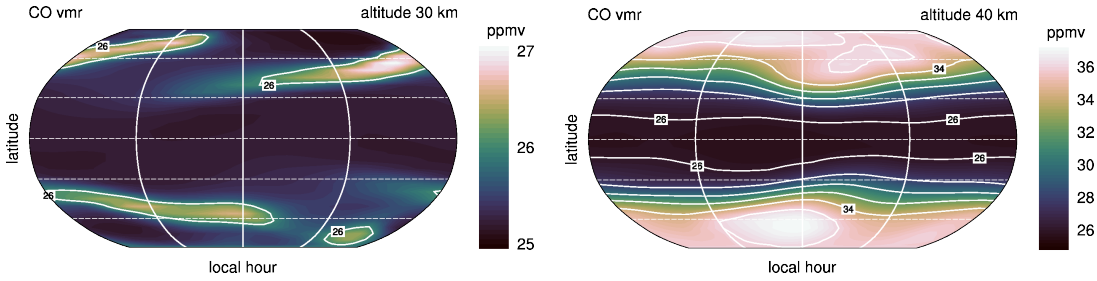

Figure 12. CO volume mixing ratio as modeled by Stolzenbach et al. (2023) at an altitude of 30 km (left) and 40 km (right). Dashed white lines indicate parallels (30° apart in latitude), and solid white lines indicate 6AM, noon and 6PM local solar times.

al., 2010; Stolzenbach et al., 2023). More specifically, the most recent 3D Venus planetary climate model including chemical processes (Stolzenbach et al., 2023) finds that, below the clouds in the 30-40 km altitude range, CO is increasing by 8 to 40% between 0° and ±60° in latitude, comparable with our observed variations of ∼ 30% (Fig. 12). Their zonally averaged vertical profile of OCS at higher latitude is also shifted downwards between ±60° and 0° by a similar amount to our observations (∼ 1.3 km compared to our ∼ 1 km). Such an interpretation supports the choice we made to parameterize OCS variations, namely by vertical shifts of its reference profile. They also find a small enhancement in water vapor at lower latitudes (30 ppmv compared to a latitudinal average of 27-28 ppmv), compatible with our observations and their uncertainties. For SO_2, their model is currently unable to reproduce an abundance of ∼ 100 ppmv below the clouds, so that it cannot yet be used to explore SO_2 chemistry below the clouds.

This interpretation of OCS variations as vertical shifts of a nominal profile could be extended to other species, so that it would be interesting to convert our CO mixing ratios variations in terms of vertical translations of the reference CO profile. This yields $\Delta z = \frac{\Delta q_{CO}}{\partial q_{CO}/\partial z} \approx \frac{10\,\mathrm{ppmv}}{1\,\mathrm{ppmv/km}} \approx 10\,\mathrm{km}$, where 1 ppmv/km is the value of the vertical CO gradient in the 30-40 km altitude range, and 10 ppmv the variations of CO between higher and lower latitudes that we observe. This equivalent 10 km vertical shift for CO is about 10 times larger than the vertical shift we observe for OCS. This highlights the fact that this altitude shift should not be understood as an actual vertical displacement (which would be common to all species), but as a more abstract quantity depending on the vertical advection, chemical relaxation time scale, local vertical gradient of the con-

sidered species, etc. Indeed, Marcq and Lebonnois (2013) found very different relaxation times for CO and OCS.

Also, the region probed in our observations is close to the deep mixed layer of which the height may reach ~ 30 km and above on some descending probe, with vertical wind of several m/s that may have measured. From the *Pioneer Venus* probes (Seiff et al., 1985), it seems that there is a strong variability of the depth of this layer with latitude and local time. *Venera* and *Pioneer Venus* probes also measured a low vertical gradient of the zonal wind between 20 and 30-35 km (Schubert et al., 1980), suggesting of a mixed layer with potentially non-negligible vertical wind. Only Baker et al. (2000) studied the small-scale turbulence in this layer, with vertical wind of speeds several m/s (Ainsworth & Herman, 1975). This would be consistent with the observed variability of minor species with a significant vertical gradient in their VMR profile, namely CO and OCS.

Finally, one can observe in our latitudinal variation pattern for both CO and OCS a significant asymmetry between the northern and southern hemisphere, already suspected by previous observers (Tsang et al., 2009; Arney et al., 2014). However, this asymmetry could be also due to the asymmetrical coverage of Venus Express, with the southern hemisphere being observed from further away but at much lower orbital speeds, and therefore co-adding over about 10 times smaller footprints – this provides a reasonable explanation for the larger statistical dispersion of measurements observed in the southern hemisphere compared to the northern hemisphere which does not resolve small scale variability. Nevertheless, if this asymmetry is genuine and in absence of significant seasonal cycles, the most likely cause for this asymmetry would be the effect of topography upon the vertical circulation, spectacularly evidenced up to cloud top by wave propagation (Piccialli et al., 2014; Fukuhara et al., 2017). Intriguingly, although the meridional-vertical circulation below the clouds modeled by Stolzenbach et al. (2023) is asymmetric with respect to the equator, their modeling of the latitudinal variations of minor species such as CO and OCS do not display a noticeable North-South asymmetry. It should also be noted that, unlike Mars, Venus zonally-averaged topography does not exhibit a significant North-South dichotomy; the only major source of North-South asymmetry being *Aphrodite Terra* centered around 20°S. We further investigate the idea of topographic influence upon observed minor species variability in the following section.

5.2 Correlations with topography

Following the work of Bertaux et al. (2016), we have looked for correlation between mean topography, and zonally-shifted CO/OCS mixing ratios at lower latitudes (below $\pm 25°$, so that we are not sensitive to the above mentioned latitudinal gradients). The result is plotted in Fig. 13. Interestingly, we find for CO a maximal correlation for a shift of about 45° in longitude, with larger values for (zonally shifted) CO above higher elevations (namely *Aphrodite Terra*), comparable with the shift value found by Bertaux et al. (2016) for cloud top level zonal winds, UV albedo and H_2O abundance in the same low latitude region. This suggests that the propagation of mountain waves interacts with the general circulation in the 30-40 km altitude range, resulting in a weaker low latitude upwelling in (zonally shifted) proximity of higher surface elevations.

Direct evidence for an influence of topography on the atmospheric waves was provided by Akatsuki, with mountain waves observed at cloud top level, preferably during the late afternoon (Kouyama et al., 2017). There are also recent observations (Encrenaz et al., 2020) and modeling (Stolzenbach et al., 2023) efforts that agree on a local minimum for cloud top SO_2 close to a longitude of 0°. Our observations of CO longitudinal variability below the clouds further strengthens the case for a direct influence of topography upon vertical motions in the Venusian troposphere (whether large scale advection or wave propagation), with a zonal shift explained by the zonal superrotation. A more quantitative assessment and interpretation would require mesoscale dynamical models (Lefèvre et al., 2020) coupled with chemical processes (including heterogeneous processes within the lower haze) at work below the clouds, which is not available yet. Coupled chemical-dynamical models exist at a planetary scale (Lebonnois et al., 2010; Stolzenbach et al., 2023) and are able to reproduce at least qualitatively the observed large scale latitudinal gradient of CO below the clouds, which gives us hope that, eventually, smaller-scale processes can be simulated too.

Fig. 13 also shows a different shift value for OCS than for CO (10° compared to 45° for CO), which is consistent for a shorter chemical relaxation time for OCS found by Marcq and Lebonnois (2013), making it a less sensitive tracer of the variations in vertical circulation induced by topography. Conversely, its steep vertical gradient (allowed by its short relaxation time) makes it better suited to monitor variations in vertical transport.

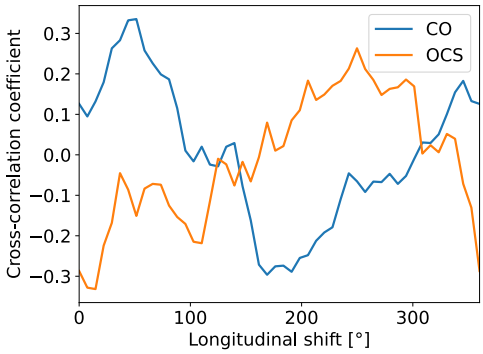

Figure 13. Cross-correlation (for latitudes below 25°) between zonally shifted surface elevation and CO mixing ratio / OCS altitude shift as a function of longitudinal shift.

6 Conclusion

The full VIRTIS-H night side 2.3 µm data set allows us to confirm and refine the previous findings about trace species variability in the troposphere (Marcq et al., 2005, 2006, 2008; Tsang et al., 2009; Arney et al., 2014), namely: (1) a 15 to 30% increase in carbon monoxide (CO) with increasing latitude between the equator and ±60° in latitude; (2) an latitudinal anti-correlation between CO and carbonyl sulfide (OCS); (3) no evidence for significant latitudinal variability for water vapor (as well as its D/H isotopic ratio) and sulfur dioxide (SO_2); (4) confirmation of the north-south asymmetry in CO and OCS variations, pointing to an orographic influence on the deep large-scale atmospheric circulation. The globally averaged values are higher than previous estimates for some species (marginally for CO in the 30-40 ppmv range at 36 km, more so for SO_2 at 190 ± 35 ppmv), but this can be explained with our updated radiative transfer model – absolute mixing ratios are notoriously harder to constrain than their spatial or temporal variations, see e.g. (Bézard et al., 2011). We were also able to discover new features in this data set, the largest so far for 2.3 µm night side spectroscopy: (1) OCS variations are better explained through vertical shifts of its abundance profile (very steep in the probed layers) rather than through a multiplicative factor, which is fully consistent with the aforementioned dynamical interpretation; (2) CO (and possibly OCS) exhibit a zonal variability at lower latitudes, correlated with the longitudinally shifted average surface elevation, yielding another hint about the influence of topography on the deep circulation.

These VIRTIS-H results highlight implicitly, through their limitations, the scientific needs for future spectroscopic measurements of the 2.3 µm window. First of all, a higher spectral resolving power ($\sim 10^4$ or higher) would allow for an enhanced accuracy on the retrievals, allowing to explore the variability of minors species other than CO and OCS, e.g. H_2O, HDO and SO_2 (Marcq et al., 2021). Also, the "dynamics vs. chemistry" interpretation of the observed spatial contrasts will require at some point a more quantitative approach, based on the use of coupled chemical models (Stolzenbach et al., 2023) which already reproduce the qualitative trends, and mesoscale/large eddy simulations currently being developed (Lefèvre et al., 2018, 2020, 2022). This, in turn, emphasizes the need to observe the spatial contrasts with a resolution of ~ 30 km (ultimately limited by the multiple scattering of the thermal emission within the cloud layers), much improved compared to VIRTIS-H (several hundreds of km).

Such improved performance is indeed expected for the payload of next generation Venus orbiters. In particular, the high resolution channel VenSpec-H of the VenSpec spectrometer suite (Helbert et al., 2019) onboard ESA's *EnVision* orbiter should be able to observe, among other spectral bands, the 2.3 µm spectral window at a spectral resolution ~ 8000 and a spatial resolution ~ 100 km. Monitoring this spectral window for a nominal duration of six Venusian years will undoubtedly yield new insights about the coupling between dynamics and chemistry below the clouds of Venus, as well as provide spatial and temporal context for the complementary in situ measurements of trace species, e.g. those planned by the Venus Tunable Laser Spectrometer (VTLS) and Venus Mass Spectrometer (VMS) during NASA's DAVINCI atmospheric probe descent (Garvin et al., 2022).

Open Research Section

VIRTIS-H data can be obtained from ESA's Planetary Science Archive (PSA) : `https://archives.esac.esa.int/psa/`. The VIRTIS/Venus Express dataset is also searchable from the Europlanet / VESPA portal (`https://vespa.obspm.fr`), cured by PADC at Paris Observatory.

Acknowledgments

EM acknowledges support from CNES and ESA for his research activities related to the VenSpec suite on board EnVision, as well as support from the INSU/Programme Na-

tional de Planétologie. SR acknowledges funding by the Belgian Science Policy Office (BELSPO) through the FED-tWIN program (Prf-2019-077 - RT-MOLEXO) and through financial and contractual support coordinated by ESA Prodex Office (PEA 4000137943, 4000128137).

References

Ainsworth, J. E., & Herman, J. R. (1975, January). Venus wind and temperature structure: The Venera 8 data. J. Geophys. Res., *80*(1), 173. doi: 10.1029/JA080i001p00173

Allen, D. A. (1987, February). The dark side of Venus. *Icarus*, *69*, 221-229.

Allen, D. A., & Crawford, J. W. (1984, January). Cloud structure on the dark side of Venus. *Nature*, *307*, 222-224.

Arney, G., Meadows, V., Crisp, D., Schmidt, S. J., Bailey, J., & Robinson, T. (2014, August). Spatially resolved measurements of H_2O, HCl, CO, OCS, SO_2, cloud opacity, and acid concentration in the Venus near-infrared spectral windows. *Journal of Geophysical Research (Planets)*, *119*, 1860-1891. doi: 10.1002/2014JE004662

Baker, R. D., Schubert, G., & Jones, P. W. (2000, January). Convectively generated internal gravity waves in the lower atmosphere of Venus. II. Mean wind shear and wave-mean flow interaction. *Journal of Atmospheric Sciences*, *57*(2), 200-215. doi: 10.1175/1520-0469(2000)057⟨0200:CGIGWI⟩2.0.CO;2

Bertaux, J.-L., Khatuntsev, I. V., Hauchecorne, A., Markiewicz, W. J., Marcq, E., Lebonnois, S., ... Fedorova, A. (2016, June). Influence of Venus topography on the zonal wind and UV albedo at cloud top level: The role of stationary gravity waves. *Journal of Geophysical Research (Planets)*, *121*(6), 1087-1101. doi: 10.1002/2015JE004958

Bézard, B., de Bergh, C., Crisp, D., & Maillard, J.-P. (1990, June). The deep atmosphere of Venus revealed by high-resolution nightside spectra. *Nature*, *345*, 508-511. doi: 10.1038/345508a0

Bézard, B., de Bergh, C., Fegley, B., Maillard, J.-P., Crisp, D., Owen, T., ... Grinspoon, D. (1993, August). The abundance of sulfur dioxide below the clouds of Venus. *Geophys. Res. Letters*, *20*, 1587-1590.

Bézard, B., Fedorova, A., Bertaux, J.-L., Rodin, A., & Korablev, O. (2011, Novem-

ber). The 1.10- and 1.18-μm nightside windows of Venus observed by SPICAV-IR aboard Venus Express. *Icarus*, *216*, 173-183. doi: 10.1016/j.icarus.2011.08.025

Bézard, B., Tsang, C. C. C., Carlson, R. W., Piccioni, G., Marcq, E., & Drossart, P. (2009, May). Water vapor abundance near the surface of Venus from Venus Express/VIRTIS observations. *Journal of Geophysical Research (Planets)*, *114*, 122-133. doi: 10.1029/2008JE003251

Carlson, R. W., Baines, K. H., Kamp, L. W., Weissman, P. R., Smythe, W. D., Ocampo, A. C., ... Grinspoon, D. (1991, September). Galileo infrared imaging spectroscopy measurements at Venus. *Science*, *253*, 1541-1548.

Collard, A. D., Taylor, F. W., Calcutt, S. B., Carlson, R. W., Kamp, L. W., Baines, K. H., ... Bézard, B. (1993, July). Latitudinal distribution of carbon monoxide in the deep atmosphere of Venus. *Planet. Space Sci.*, *41*, 487-494. doi: 10.1016/0032-0633(93)90033-X

Coradini, A., Capaccioni, F., Drossart, P., Semery, A., Arnold, G., Schade, U., ... Tozzi, G. (1998, October). VIRTIS : an imaging spectrometer for the ROSETTA mission. *Planet. Space Sci.*, *46*, 1291-1304.

Cotton, D. V., Bailey, J., Crisp, D., & Meadows, V. S. (2012, February). The distribution of carbon monoxide in the lower atmosphere of Venus. *Icarus*, *217*, 570-584. doi: 10.1016/j.icarus.2011.05.020

Crisp, D. (1986, September). Radiative forcing of the Venus mesosphere. I - Solar fluxes and heating rates. *Icarus*, *67*, 484-514. doi: 10.1016/0019-1035(86)90126-0

Crisp, D., Sinton, W. M., Hodapp, K.-W., Ragent, B., Gerbault, F., & Goebel, J. H. (1989, October). The nature of the near-infrared features on the Venus night side. *Science*, *246*, 506-509.

de Bergh, C., Bézard, B., Crisp, D., Maillard, J. P., Owen, T., Pollack, J., & Grinspoon, D. (1995, April). Water in the deep atmosphere of Venus from high-resolution spectra of the night side. *Advances in Space Research*, *15*, 79-88.

de Bergh, C., Bézard, B., Owen, T., Crisp, D., Maillard, J.-P., & Lutz, B. L. (1991, February). Deuterium on Venus - Observations from earth. *Science*, *251*, 547-549.

Drossart, P., Piccioni, G., Adriani, A., Angrilli, F., Arnold, G., Baines, K. H., ...

Afanasenko, T. Z. (2007, October). Scientific goals for the observation of Venus by VIRTIS on ESA/Venus express mission. Planet. Space Sci., *55*(12), 1653-1672. doi: 10.1016/j.pss.2007.01.003

Encrenaz, T., Greathouse, T. K., Marcq, E., Sagawa, H., Widemann, T., Bézard, B., ... Bierson, C. J. (2020, July). HDO and SO_2 thermal mapping on Venus. V. Evidence for a long-term anti-correlation. A&A, *639*, A69. doi: 10.1051/0004-6361/202037741

Fedorova, A., Bézard, B., Bertaux, J.-L., Korablev, O., & Wilson, C. (2015, August). The CO_2 continuum absorption in the 1.10- and 1.18-μm windows on Venus from Maxwell Montes transits by SPICAV IR onboard Venus express. Planet. Space Sci., *113*, 66-77. doi: 10.1016/j.pss.2014.08.010

Fukuhara, T., Futaguchi, M., Hashimoto, G. L., Horinouchi, T., Imamura, T., Iwagaimi, N., ... Yamazaki, A. (2017, January). Large stationary gravity wave in the atmosphere of Venus. *Nature Geoscience*, *10*(2), 85-88. doi: 10.1038/ngeo2873

Garvin, J. B., Getty, S. A., Arney, G. N., Johnson, N. M., Kohler, E., Schwer, K. O., ... Zolotov, M. (2022, May). Revealing the Mysteries of Venus: The DAVINCI Mission. *The Planetary Science Journal*, *3*(5), 117. doi: 10.3847/PSJ/ac63c2

Grinspoon, D. H. (1993, June). Implications of the high D/H ratio for the sources of water in Venus' atmosphere. *Nature*, *363*, 428-431. doi: 10.1038/363428a0

Hansen, J. E., & Hovenier, J. W. (1974, May). Interpretation of the polarization of Venus. *Journal of Atmospheric Sciences*, *31*, 1137-1160. doi: 10.1175/1520-0469(1974)031⟨1137:IOTPOV⟩2.0.CO;2

Haus, R., Kappel, D., & Arnold, G. (2015, January). Lower atmosphere minor gas abundances as retrieved from Venus Express VIRTIS-M-IR data at 2.3 μm. Planet. Space Sci., *105*, 159-174. doi: 10.1016/j.pss.2014.11.020

Helbert, J., Vandaele, A. C., Marcq, E., Robert, S., Ryan, C., Guignan, G., ... Lara, L. (2019, September). The VenSpec suite on the ESA EnVision mission to Venus. In M. Strojnik & G. E. Arnold (Eds.), *Infrared remote sensing and instrumentation xxvii* (Vol. 11128, p. 1112804). doi: 10.1117/12.2529248

Huang, X., Gamache, R. R., Freedman, R. S., Schwenke, D. W., & Lee, T. J. (2014). Reliable infrared line lists for 13 CO_2 isotopologues up to $E' = 18,000$ cm^{-1}

and 1500 K, with line shape parameters. J. Quant. Spec. Radiat. Transf., *147*, 134-144. Retrieved from https://www.sciencedirect.com/science/article/pii/S0022407314002246 doi: https://doi.org/10.1016/j.jqsrt.2014.05.015

Jacquinet-Husson, N., Crepeau, L., Armante, R., Boutammine, C., Chédin, A., Scott, N. A., ... Vander Auwera, J. (2011, November). The 2009 edition of the GEISA spectroscopic database. J. Quant. Spec. Radiat. Transf., *112*, 2395-2445. doi: 10.1016/j.jqsrt.2011.06.004

Khatuntsev, I. V., Patsaeva, M. V., Titov, D. V., Ignatiev, N. I., Turin, A. V., Limaye, S. S., ... Moissl, R. (2013, September). Cloud level winds from the Venus Express Monitoring Camera imaging. *Icarus*, *226*, 140-158. doi: 10.1016/j.icarus.2013.05.018

Kouyama, T., Imamura, T., Taguchi, M., Fukuhara, T., Sato, T. M., Yamazaki, A., ... Nakamura, M. (2017, December). Topographical and Local Time Dependence of Large Stationary Gravity Waves Observed at the Cloud Top of Venus. Geophys. Res. Lett., *44*(24), 12,098-12,105. doi: 10.1002/2017GL075792

Lebonnois, S., Hourdin, F., Eymet, V., Crespin, A., Fournier, R., & Forget, F. (2010, June). Superrotation of Venus' atmosphere analyzed with a full general circulation model. *Journal of Geophysical Research (Planets)*, *115*, 6006. doi: 10.1029/2009JE003458

Lefèvre, M., Lebonnois, S., & Spiga, A. (2018, October). Three-Dimensional Turbulence-Resolving Modeling of the Venusian Cloud Layer and Induced Gravity Waves: Inclusion of Complete Radiative Transfer and Wind Shear. *Journal of Geophysical Research (Planets)*, *123*(10), 2773-2789. doi: 10.1029/2018JE005679

Lefèvre, M., Marcq, E., & Lefèvre, F. (2022, November). The impact of turbulent vertical mixing in the Venus clouds on chemical tracers. Icarus, *386*, 115148. doi: 10.1016/j.icarus.2022.115148

Lefèvre, M., Spiga, A., & Lebonnois, S. (2020, January). Mesoscale modeling of Venus' bow-shape waves. Icarus, *335*, 113376. doi: 10.1016/j.icarus.2019.07.010

Marcq, E., Amine, I., Duquesnoy, M., & Bézard, B. (2021, April). Evidence for SO_2 latitudinal variations below the clouds of Venus. A&A, *648*, L8. doi: 10.1051/

675 0004-6361/202140837

676 Marcq, E., Bézard, B., Drossart, P., Piccioni, G., Reess, J. M., & Henry, F. (2008,
677 September). A latitudinal survey of CO, OCS, H_2O, and SO_2 in the lower
678 atmosphere of Venus: Spectroscopic studies using VIRTIS-H. *Journal of Geo-*
679 *physical Research (Planets)*, *113*, 0-+. doi: 10.1029/2008JE003074

680 Marcq, E., Bézard, B., Encrenaz, T., & Birlan, M. (2005, December). Latitu-
681 dinal variations of CO and OCS in the lower atmosphere of Venus from
682 near-infrared nightside spectro-imaging. *Icarus*, *179*, 375-386. doi:
683 10.1016/j.icarus.2005.06.018

684 Marcq, E., Encrenaz, T., Bézard, B., & Birlan, M. (2006, November). Remote
685 sensing of Venus' lower atmosphere from ground-based IR spectroscopy: Lat-
686 itudinal and vertical distribution of minor species. *Planet. Space Sci.*, *54*,
687 1360-1370. doi: 10.1016/j.pss.2006.04.024

688 Marcq, E., Lea Jessup, K., Baggio, L., Encrenaz, T., Lee, Y. J., Montmessin, F.,
689 ... Bertaux, J.-L. (2020, January). Climatology of SO_2 and UV absorber at
690 Venus' cloud top from SPICAV-UV nadir dataset. Icarus, *335*, 113368. doi:
691 10.1016/j.icarus.2019.07.002

692 Marcq, E., & Lebonnois, S. (2013, October). Simulations of the latitudinal variabil-
693 ity of CO-like and OCS-like passive tracers below the clouds of Venus using
694 the Laboratoire de Météorologie Dynamique GCM. *Journal of Geophysical*
695 *Research (Planets)*, *118*, 1983-1990. doi: 10.1002/jgre.20146

696 Marcq, E., Mills, F. P., Parkinson, C. D., & Vandaele, A. C. (2018, February). Com-
697 position and Chemistry of the Neutral Atmosphere of Venus. Space Sci. Rev.,
698 *214*(1), 10. doi: 10.1007/s11214-017-0438-5

699 Markiewicz, W. J., Titov, D. V., Ignatiev, N., Keller, H. U., Crisp, D., Limaye,
700 S. S., ... Matz, K. D. (2007, October). Venus Monitoring Camera for Venus
701 Express. Planet. Space Sci., *55*(12), 1701-1711. doi: 10.1016/j.pss.2007.01.004

702 Newville, M., Otten, R., Nelson, A., Stensitzki, T., Ingargiola, A., Allan, D., ...
703 Hahn, A. (2022, November). *lmfit/lmfit-py: 1.0.4rc1.* Zenodo. Retrieved from
704 `https://doi.org/10.5281/zenodo.7343457` doi: 10.5281/zenodo.7343457

705 Peralta, J., Sánchez-Lavega, A., Horinouchi, T., McGouldrick, K., Garate-Lopez, I.,
706 Young, E. F., ... Limaye, S. S. (2019, November). New cloud morphologies
707 discovered on the Venus's night during Akatsuki. Icarus, *333*, 177-182. doi:

10.1016/j.icarus.2019.05.026

Piccialli, A., Titov, D. V., Sanchez-Lavega, A., Peralta, J., Shalygina, O., Markiewicz, W. J., & Svedhem, H. (2014, January). High latitude gravity waves at the Venus cloud tops as observed by the Venus Monitoring Camera on board Venus Express. *Icarus*, *227*, 94-111. doi: 10.1016/j.icarus.2013.09.012

Pollack, J. B., Dalton, J. B., Grinspoon, D., Wattson, R. B., Freedman, R., Crisp, D., ... Tipping, R. (1993, May). Near-infrared light from Venus' nightside - A spectroscopic analysis. *Icarus*, *103*, 1-42. doi: 10.1006/icar.1993.1055

Schubert, G., Covey, C., del Genio, A., Elson, L. S., Keating, G., Seiff, A., ... von Zahn, U. (1980, December). Structure and circulation of the Venus atmosphere. J. Geophys. Res., *85*, 8007-8025. doi: 10.1029/JA085iA13p08007

Seiff, A. (1983). Thermal structure of the atmosphere of Venus. In S. W. Bougher, D. M. Hunten, & R. S. Phillips (Eds.), *Venus* (p. 215-279). University of Arizona Press, Tucson.

Seiff, A., Schofield, J. T., Kliore, A. J., Taylor, F. W., Limaye, S. S., Revercomb, H. E., ... Marov, M. Y. (1985, January). Models of the structure of the atmosphere of Venus from the surface to 100 kilometers altitude. *Advances in Space Research*, *5*(11), 3-58. doi: 10.1016/0273-1177(85)90197-8

Stamnes, K., Tsay, S., Jayaweera, K., & Wiscombe, W. (1988, June). Numerically stable algorithm for discrete-ordinate-method radiative transfer in multiple scattering and emitting layered media. Appl. Opt., *27*, 2502-2509.

Stolzenbach, A., Lefèvre, F., Lebonnois, S., & Määttänen, A. (2023, May). Three-dimensional modeling of Venus photochemistry and clouds. Icarus, *395*, 115447. doi: 10.1016/j.icarus.2023.115447

Titov, D. V., Ignatiev, N. I., McGouldrick, K., Wilquet, V., & Wilson, C. F. (2018, December). Clouds and Hazes of Venus. Space Sci. Rev., *214*(8), 126. doi: 10.1007/s11214-018-0552-z

Titov, D. V., Svedhem, H., McCoy, D., Lebreton, J.-P., Barabash, S., Bertaux, J.-L., ... Coradini, M. (2006, July). Venus Express: Scientific goals, instrumentation, and scenario of the mission. *Cosmic Research*, *44*, 334-348. doi: 10.1134/S0010952506040071

Tsang, C. C. C., Irwin, P. G. J., Wilson, C. F., Taylor, F. W., Lee, C., de Kok, R.,

... Calcutt, S. (2008, October). Tropospheric carbon monoxide concentrations and variability on Venus from Venus Express/VIRTIS-M observations. *Journal of Geophysical Research (Planets)*, *113*, 0. doi: 10.1029/2008JE003089

Tsang, C. C. C., & McGouldrick, K. (2017, June). General circulation of Venus from a long-term synoptic study of tropospheric CO by Venus Express/VIRTIS. Icarus, *289*, 173-180. doi: 10.1016/j.icarus.2017.02.018

Tsang, C. C. C., Taylor, F. W., Wilson, C. F., Liddell, S. J., Irwin, P. G. J., Piccioni, G., ... Calcutt, S. B. (2009, June). Variability of CO concentrations in the Venus troposphere from Venus Express/VIRTIS using a Band Ratio Technique. Icarus, *201*(2), 432-443. doi: 10.1016/j.icarus.2009.01.001

Yamazaki, A., Yamada, M., Lee, Y. J., Watanabe, S., Horinouchi, T., Murakami, S.-y., ... Nakamura, M. (2018, 12). Ultraviolet imager on venus orbiter akatsuki and its initial results. *Earth, Planets and Space*, *70*. doi: 10.1186/s40623-017-0772-6